Volume 1 | Number 1 | Jan 2013 | Pages 1–100

PCCP

Physical Chemistry Chemical Physics
www.rsc.org/pccp

ROYAL SOCIETY OF CHEMISTRY

ROYAL SOCIETY OF CHEMISTRY

www.rsc.org/pccp

Hydrogen-bonded ring closing and opening of protonated methanol clusters

$H^+(CH_3OH)_n$ (n = 4 - 8) with the inert gas tagging

Ying-Cheng Li,[1][‡] Toru Hamashima,[2][‡] Ryoko Yamazaki,[2] Tomohiro Kobayashi,[2]

Yuta Suzuki,[2] Kenta Mizuse,[2][†] Asuka Fujii,[2]* Jer-Lai Kuo[1]*

Institute of Atomic and Molecular Sciences, Academia Sinica, Taipei, 10617, Taiwan

Department of Chemistry, Graduate School of Science,

Tohoku University, Sendai 980-8578, Japan

* To whom corresponding should be addressed.

E-mail: asukafujii@m.tohoku.ac.jp (A.F.), jlkuo@pub.iams.sinica.edu.tw (J.-L.K.).

[1] Academia Sinica

[2] Tohoku University

[‡] Ying-Chen Li and Toru Hamashima contributed equally to this study.

[†] Present address Tokyo Institute of Technology, Tokyo, 152-8551 Japan

1

Abstract

The preferential hydrogen bond (H-bond) structures of the protonated methanol clusters, $H^+(MeOH)_n$, in the size range of $n = 4 - 8$, were studied by size-selective infrared (IR) spectroscopy in conjunction with density functional theory calculations. The IR spectra of the bare clusters were compared with those with the inert gas tagging by Ar, Ne, and N_2, and remarkable changes of the isomer distribution with the tagging were found in $n \geq 5$. The temperature dependence of the isomer distribution of the clusters was calculated by the quantum harmonic superposition approach. The observed spectral changes with the tagging were well interpreted by the fall of the cluster temperature with the tagging, which causes the transfer of the isomer distribution from the open and flexible H-bond network types to the closed and rigid ones. Anomalous isomer distribution with the tagging, which has been recently found for protonated water clusters, was also found for $H^+(MeOH)_5$. The origin of the anomaly was examined by the experiments on its carrier gas dependence.

I.INTRODUCTION

In gas phase experimental studies on charged clusters, e.g., protonated clusters of protic molecules, charged clusters are usually generated with large excess energy. Their vibrational temperature is typically 150 ~ 200 K or higher even after the jet expansion cooling, and preparation of cold (< ~100 K) clusters is rather difficult. [1-9] Though the minimum energy structure tends to the focus in spectroscopic studies of clusters, the most preferred structure actually depends on the vibrational temperature of the cluster because higher energy structures can be dominant by the temperature-dependent entropy factor in the free energy. [10-11] Therefore, vibrational temperature (or vibrational energy) dependence of cluster structures has recently attracted great interest, especially for charged clusters.

For control of the vibrational temperature (or vibrational energy) of charged clusters, collisional cooling or rare gas "tagging" has been employed. [2, 12-29] The former technique utilizes collisions with temperature-controlled buffer gas in the ion trap. The latter simply restricts the upper limit of the vibrational energy by the weak intermolecular bond with a rare gas atom (or an inert diatomic molecule such as H_2 and N_2). The combination of these two techniques has also recently been employed to obtain a high and constant dissociation yield in dissociation spectroscopy of clusters in a

3

cold ion-trap.[16-19, 25]   Temperature or vibrational energy dependence of structures has

been reported particularly for charged clusters including water molecules.[1-5, 8-11, 16-19,

22-29]   Unexpected preference of isomer structures, which deviates from the assumption

of the simple thermal equilibrium, has been found for the water network with the

tagging, and its origin has not yet been fully clarified. [4, 30-36]

Methanol is also a typical protic solvent, and hydrogen-bond (H-bond) network

structures of protonated methanol clusters, $H^+(MeOH)_n$, have been studied by infrared

(IR) spectroscopy and density functional theory (DFT) calculations. [7, 37-45] One of the

important features of the H-bond networks of $H^+(MeOH)_n$ is their simplicity. We have

shown that there only exist 6 types in the H-bond network morphology of $H^+(MeOH)_n$.

[39, 40]   In $n \leq 3$, only linear (chain) type structures are possible for $H^+(MeOH)_n$.   In $n \geq$

4, cyclic (or cyclic with a side chain) type structures can be formed, and they compete

with linear type isomers.   At $n = 5$, coexistence of linear and cyclic isomers has been

reported by Chang *et al.*; while only the higher energy linear isomer was observed with

the jet expansion under the low stagnation pressure, the rise of the IR spectral signature

of the lower energy cyclic isomer was observed with increase of the stagnation pressure.

[37, 38]   In $n \geq 7$, the more compact structures, bicyclic (multiple ring) type structures, are

plausible.   These bicyclic structures are the terminal in the development of the H-bond

network morphology of $H^+(MeOH)_n$, and more complicated H-bond networks cannot be constructed. Because of this simplicity of the H-bond networks, we expect that temperature dependence of the preferred H-bond network of protonated methanol clusters is simple and clear. In our previous paper, we reported that the complete switching of the isomer distribution of $H^+(MeOH)_7$ from the higher energy linear isomers to the lower energy bicyclic isomers occurs with the Ar and Ne tagging. [7] The isomer distribution simulations based on the quantum harmonic superposition approximation (Q-HSA) well reproduced the observed switching in terms of the fall of the temperature from 150 - 200 K to ~50 K. This was consistent with the upper limit evaluation of the vibrational temperature of the cluster under the Ar or Ne tagging. Recently Fifen *et al*. attempted to find structures of $H^+(MeOH)_n$ ($n = 4 - 9$) under a continuous medium with dielectric constant of methanol, and they predicted the relative stabilities of a few selected isomers.[44, 45] These previous studies suggest that protonated methanol clusters are a very suitable model system to examine temperature dependence of microscopic H-bonded network structures, though their experimental confirmation has not yet been systematically performed. [7, 37, 38]

In the present paper, we report the comprehensive study on the H-bond network changes of $H^+(MeOH)_n$ induced by the inert gas tagging in the size range of $n = 4 - 8$.

We observe size-selective IR spectra of the clusters in the OH stretching vibrational region with and without tags. Ar, Ne, and N_2 are used as tag species. Spectral simulations based on Q-HSA are compared with the observed spectra and spectral changes by the tagging are interpreted by the temperature dependence of the isomer distribution. With this systematic study in the various cluster size, we establish the general trend of temperature dependence of the microscopic H-bond networks.

In addition, we report remarkable isomer selectivity in the tagging of $n = 5$, that cannot be explained simply by the magnitude of the intermolecular interaction between the cluster and tag. This anomaly is quite similar to the isomer selectivity found in the tagging of $H^+(H_2O)_n$. [32-35] Additional experiments are performed and the origin of the isomer selectivity is discussed.

II. EXPERIMENTAL SECTION

The experimental schemes used in this study are shown in Figure 1. [32] $H^+(MeOH)_n$ clusters were produced by a supersonic jet expansion of the gaseous mixture of methanol/(tag species)/carrier and electron ionization of -200 V at the collisional region. The total stagnation pressure of the gaseous mixture was typically 9 MPa, and the methanol concentration was ~0.1%. $H^+(MeOH)_n$-X (X = Ar, Ne, N_2 and H_2) tagged

6

clusters were also produced by the expansion of the gaseous mixture and the electron

ionization. Concentration of the tag species in the gaseous mixture was ~100% (carrier

gas itself is the tag species) in the Ne tag and was ~5% in the other tags.   Carrier gas

was He or Ar. For each observed IR spectrum, the constituents of the gaseous mixture

will be indicated at the figure caption. The cluster of interest was mass-selected by a

quadrupole mass filter and was introduced into an octopole ion guide.

Counter-propagating coherent IR light was introduced into the ion guide, and fragment

ions produced by vibrational predissociation were detected by the second quadrupole

mass filter.   The $H^+(MeOH)_{n-1}$ fragment (MeOH-loss channel) was monitored to

measure IR spectra of bare $H^+(MeOH)_n$ while the $H^+(MeOH)_n$ fragment (X-loss

channel) was monitored to measure spectra of the tagged clusters. Coherent IR light was

generated by an IR optical parametric oscillator/amplifier (Laser Vision) pumped with

the fundamental output of a YAG laser (Spectra Physics, GCR230). All the observed

spectra were normalized according to the IR power and were calibrated to the vacuum

wavenumber by simultaneous observation of atmospheric water absorption lines.

III. CALCULATION SECTION

Structures of $H^+(MeOH)_n$ were studied previously by some of us based on the evolution

of its H-bonded networks. [40] In this work, we apply a first-principles based multi-model

method proposed by Nguyen *et al.* to systematically search the local minimum

structures of $H^+(MeOH)_n$ so that conformational isomers within a H-bond

morphological groups can be faithfully represented. [46-48] All structurally distinct isomers

we identified using empirical models were first re-optimized by using

B3LYP/6-31+G(d). This level of theory and basis set were chosen because of its

computational efficiency and reasonable accuracy. The latter has extensively been

demonstrated by Chang and co-workers in protonated H-bonded clusters by comparing

with their experimental IR spectral data.[1, 37, 49-51] The importance of the dispersion

correction in the evaluation of the absolute binding energy has been demonstrated for

the protonated methanol clusters by Fifen and co-workers. [44] As for relative energies

among structural isomers, however, the reasosonable accuracy of the B3LYP/6-31+G(d)

level evaluation has been confirmed by the comaprison with the dispersion-corrected

DFT method. [6, 7] In the present study, we only utlize relative energies for temperature

dependence calculations of isomer population. Details of the confirmation in the

present system by comparison with the ωB97X-D/6-311++G(3df,3pd) level calculations

are summarized in Electronic Supplementary Information (ESI).

In this work, all calculated IR spectra and relative energetics of different structural isomers $H^+(MeOH)_n$ are based on B3LYP/6-31+G(d). In our previous work, Gibbs free energies were selected to compare their relative energetics at finite temperature. [40] In the present atudy, to consider the contribution of all structural isomers, we used Q-HSA to sum up their thermal contributions. [6-8] IR spectrum intensity can be expressed as $I_{total}(\omega,T)=\Sigma_a I_a(\omega)P_a(T)$, where the $I_a(\omega)$ and $P_a(T)$ are the spectral intensity and statistical population weights of a-th isomer, respectively. In all DFT-calculated IR spectra, harmonic frequencies are rescaled by a factor of 0.973. The scaling factor is determined to reproduce the free OH stretch bands of the clusters. For the homogeneous width, we brodened free OH and CH streching modes with 20 and 5 cm^{-1}, respectively. For the width of H-bonded OH stretching, we adopted a power law formula $(\Gamma=\alpha(\omega_{freeOH}-\omega)^{\beta})$ proposed by Takahashi and co-worker. [52, 53] To be consistent with our previous work, we used the same value with $\alpha = 0.0009$, $\beta = 1.9$ and $\omega_{freeOH} = 3678$ cm^{-1}. [7] All the density functional theory calculations were done using the Gaussian 09 program package. [54]

As dispersion interaction is expected to play an important role in the binding of tagging atoms/molecules to $H^+(MeOH)_n$, we re-optimized selected low-energy isomers using ωB97X-D/6-311++G(3df,3pd) and then ωB97X-D/6-311++G(3df,3pd) was

engaged exclusively to search for the binding sites and evaluate the binding energies of

taggs to $H^+(MeOH)_n$. The upper limit of the vibrational temperature (T_{max}) of the

tagged cluster is evaluated by assuming that the thermal vibrational energy is lower than

the binding energy with the tag (D_e). [7] From statistical thermodynamics, the partition

function of a set of harmonic oscillators can be expressed as

$$q_{vib} = \prod_{j=1}^{k}\sum_{n=0}^{\infty}e^{-\beta E_{j,n}} = \prod_{j=1}^{k}\sum_{n=0}^{\infty}e^{-\beta h\nu_j(n+\frac{1}{2})} = \prod_{j=1}^{k}\frac{e^{-\frac{1}{2}\beta h\nu_j}}{1-e^{-\beta h\nu_j}}$$ The total vibrational energy can be

written as $U_{vib}^{total} = -\frac{\partial}{\partial\beta}\ln(q_{vib}) = \sum_{j=1}^{k}\frac{1}{2}h\nu_j + \frac{h\nu_j}{e^{\beta h\nu_j}-1}$, where the first term of U_{vib} is

the zero-point energy and the second term of U_{vib} is the thermal vibrational energy

(E_{vib}). Thus, the E_{vib} as a function of the inverse vibrational temperature $\beta \ (\equiv 1/k_B T)$ is

given as $E_{vib} = \sum_{j=1}^{k}\frac{h\nu_j}{e^{\beta h\nu_j}-1}$, where $h\nu_j$ is the vibrational energy of the j-th

vibrational normal mode, k is the total number of vibrational normal mode which is

equal to $3N$-6. T_{max} is the temperature at which the thermal vibrational energy is

equal to the binding energy with the tag.

IV. RESULTS AND DISCUSSION

1. H-bond network structure types in $H^+(MeOH)_n$ and their temperature

dependence

Prior to presentation of experimental and calculation results, we review the H-bond network "morphology" in $H^+(MeOH)_n$. This has been discussed in our previous papers, and here we briefly summarize the results for convenience in the following discussion. [39, 40] The schematic representations of the H-bond network are shown in Figure 2. In these schemes, a circle shows a methanol molecule.   The simplest network is the linear (**L**) type. The protonated ion core $CH_3OH_2^+$ (or the Zundel type core $H^+(CH_3OH)_2$) is located at the center of the network, and it becomes a double donor (DD) site. Two 1-dimensional H-bond chains are extended from the core.   Each chain is terminated by a 1-coordinated (single acceptor, A) site which has a free OH group. When a chain in the **L** type extends, it can be bound to the other end, and the network develops into the cyclic (**C**) type.   In the **C** type network, a new binding site with double acceptor (AA) site still has a free OH group. The DFT simulations have shown that stable **C** type can found in $n \geq 4$.   A 1-dimensional chain ("tail") can be further extended from this AA site (then this AA site becomes a double acceptor single donor, AAD, site), and such a structure is called cyclic with a tail (**Ct**).   The **Ct** type can emerge in $n \geq 5$.   Since the terminal of the "tail" in **Ct** is an A site, the "tail" moiety can be bound to somewhere on the ring moiety to form another ring.   Then, the

bicyclic (**bC**) type is formed. This **bC** type is the most compact network in $H^+(MeOH)_n$. The **bC** type has no free OH group, and this should be a spectral signature of the **bC** type. The **bC** type can be stable in $n \geq 5$. Further development is limited to expansion of the ring size and attachment of side chains to the ring moiety. Such a side chain is terminated by a single donor site and it cannot be bound to the ring moiety to form more complicated 3-dimensional network. Therefore, the **bC** type is the terminal in the topological development of the H-bond networks in $H^+(MeOH)_n$.

For illustration purposes, structures of the most stable isomers of each morphological type for $n = 4$ to 8 are also shown in Fig. 2. In our early studies, relative stabilities of different morphological group for a given temperature were estimated by computing the Gibbs free energy of these representative isomers.[40] However, it is important to point out here that there are different numbers of conformational isomers within each topological type for a given size. For a more faithful description on thermal behavior at elevated temperatures, it is required to include all isomers of comparable free energies.[7, 55] The numbers of conformational distinct isomers for $n = 4$ to 8 in our search are compiled in Table SI (in ESI). In the following discussion, thermal averaging is always performed by summing up the contribution from all isomers according to their statistical weights.

The calculated relative population of each morphological type is summarized in Figure 3. In our previous study on $H^+(MeOH)_7$, we have found **C** and **Ct** share similar temperature region of thermal stability.[7] Since we report simulation results for various sizes, we group both **C** and **Ct** together in Figure 3 for simplicity. We can find that **L** type isomers dominate the whole temperature range for $n = 4$. In $n = 5$ and $n = 6$, cyclic (both **C** and **Ct**) type isomers are energetically more favorable and remain as minimum in free energy until around 125 K (for $n = 5$) and 160 K (for $n = 6$) before the high energy **L** type takes over. For $n = 7$ and $n = 8$, two structural changes driven by temperature can be seen. At these sizes, the **bC** isomers, the terminal morphology, are energetically most stable and they survive up to ~ 100 K. Above this temperature, **C** and **Ct** are the most abundant group. At even higher temperatures, the **L** type isomers finally take over. Here we note that the recent theoretical work by Fifen *et al*. has showed the basically similar trend of the temperature dependence.[45] However, the isomer switching temperature is very different in their calculations, and part of the isomer population behavior clearly conflicts with the present result (for example, in $n = 5$, the **L** type isomer is predicted to be most favored in all the temperature and the population switching from **C** to **L** does not occur in their calculation). As shown in later, the present calculations well reproduce the observed spectral changes with the tagging, and

this indicates high reliability of the present theoretical calculations.   The origin of the

difference between the present calculations and those by Fifen *et al*. will be discussed

again in Sec. IV 7.

In the next section, we will discuss the temperature dependence of IR spectral

features as the evidence of above-mentioned structural changes. In Figure 3, we use

dash lines to highlight two characteristic temperatures at 50 K and 200 K. In the former,

it is clear that the populations are dominate by low-energy minima and in our previous

work on $H^+(MeOH)_7$, good agreement between our simulated IR spectrum and

Ar-tagged experimental spectrum was found at this temperature. [7] For the bare cluster,

the temperature range between 150 K and 200 K is a reasonable estimate in many

previous works on protonated water and methanol clusters produced in a jet. [1, 2, 7 8]

2. Gross features of the observed IR spectra and comparison with the simulations

Figure 4 show observed IR spectra of (b) bare and (d) Ar-tagged $H^+(MeOH)_n$ clusters (*n*

= 4 – 8) in the OH and CH stretching vibrational region along with simulated IR spectra

at (a) 50 and (c) 200 K.   The upper traces show the full frequency region (2430 – 3840

cm^{-1}), and the lower traces are the expanded plots of the high frequency region (3200 –

3840 cm^{-1}).   The observed spectra of the bare clusters are essentially the same as those

reported in our early studies, though the quality of the spectra shown here is much

improved. [39]   In addition, the jet expansion conditions are largely changed and this

might cause some minor differences.   The Ar-tagged spectrum of $n = 7$ has also been

reported in one of our previous papers. [7]

In the observed IR spectra, the relatively sharp peaks above 3600 cm^{-1} are

assigned to free OH stretch vibrations.   The bands below 3600 cm^{-1} are attributed to

H-bonded OH stretching vibrations.   Some features in the 2800 – 3000 cm^{-1} region are

CH stretch bands and they are overlapped with the broadened OH stretch bands.   In all

the cluster sizes, narrowing of band widths is clearly seen in the Ar tagged spectra, and

this is attributed to the suppression of hot band components with the tagging.

Moreover, especially in $n = 5 – 8$, disappearance of some bands and appearance of new

bands are clearly seen upon the tagging.   These remarkable spectral changes suggest

that the isomer distributions are largely influenced by the tagging.

When the observed spectra of the bare and Ar tagged clusters are compared

with the simulated spectra at 200 and 50 K, respectively, we find the observed spectral

changes upon the tagging are reproduced very well by the fall of the temperature in the

simulation.   This is conspicuous, *e.g.*, in the disappearance of the free OH band in $n =$

7 and 8 and appearance of new bands at around ~3450 cm^{-1} in $n = 5, 7,$ and 8.   Though

details in each size will be discussed in the following sections, the comparison of the

observed and simulated spectra shown in Figure 4 clearly demonstrates that the isomer

population switching is essential in the spectral changes upon the tagging.

Experimental spectra of the Ne and N_2 tags are shown with those of the

corresponding bare and Ar tagged clusters in Figure 5. The upper traces show the full

observed frequency region (2430 – 3840 cm^{-1}), and the lower traces are the expanded

plots of the high frequency region (3200 – 3840 cm^{-1}). The three tagged spectra are

similar to each other at n = 4 and 6 - 8. In these sizes, no clear tag dependence of the

isomer distribution (isomer selectivity by tags) is found. However, in n = 5, the Ne

tagged spectrum is clearly different from the Ar and N_2 tagged spectra. This isomer

preference of the Ne tag cannot be simply interpreted by the energetics (temperature)

and it will be examined in detail later.

3. n = 4 cluster

In the spectrum of the bare cluster of n = 4 shown in Figures 4 and 5, a much broadened

H-bonded OH stretch band is seen in below 3500 cm^{-1} and some features due to CH

stretches are overlapped at around 3000 cm^{-1}. A relatively sharp band of the free OH

stretches appears at 3673 cm^{-1}. This spectrum is essentially the same as that

previously reported by Chang *et al*. [37, 38] They have attributed to the spectrum to an **L**

type isomer of n = 4. The **L** type structure has been also suggested to the analogue

16

system, protonated ethanol cluster $H^+(CH_3CH_2OH)_4$. [56] In $n = 4$, the spectral changes

upon the tagging are small. The spectral features are essentially kept, but the peak

position of the broadened H-bonded OH band is shifted to lower frequency by ~200

cm^{-1} upon the tagging. The three tagged spectra are similar to each other, but only

the N_2 tagged spectrum shows two free OH bands. One (3673 cm^{-1}) is the same as the

free OH band seen in the two other tagged clusters (3676 and 3678 cm^{-1} in the Ar and

Ne tags, respectively) and the bare cluster. The other band (3645 cm^{-1}) is shifted to

lower frequency and its intensity is largely enhanced. These two free OH bands in the

N_2 tagged spectrum are well interpreted by **L** type isomers which have a free OH in

each terminal of the H-bonded chains. In the bare cluster, the stretching frequencies of

the two free OH groups are degenerated. Upon the tagging, the N_2 tag is H-bonded to

one of the terminal and it will cause a frequency shift and intensity enhancement of the

OH stretch band. In the Ar and Ne tagging, the tag atom does not necessarily attach to

the terminal OH and the attachment to the protonated site is rather probable. This

different behavior of the tagging site is rationalized by the large difference of the proton

affinity of N_2 (494 kJ/mol) from those of Ar (369 kJ/mol) and Ne (199 kJ/mol). [57]

For $n = 4$, in addition to **L**, the **C** type isomer is also stable. There is, however,

only one free OH (AA site) in the **C** type isomer and this cannot explain the splitting in

the N_2 tag.   Therefore, the band splitting in the N_2-tagged spectrum evidences the **L**

type isomer.   We confirmed that tagging by two N_2 molecules results in a single free

OH peak at 3647 cm^{-1} (see the Electronic Supplementary Information).   This means

that both the terminal free OHs are bound to N_2 and their frequencies are shifted by the

same magnitude.   This observation is also consistent with the exclusive distribution of

the **L** type isomer.

In $n = 4$, the **L** type isomer is more stable than the **C** type.   In addition, the **L**

type is more flexible than the **C** type and has lower-frequency intermolecular vibrational

modes. Therefore, the **L** type has lower free energy than the **C** type even with the

elevation of temperature.   As expected by this qualitative discussion, the SHA

simulation shown in Figure 3 predicts that the **L** type isomer is exclusive in all the

temperature range.   This result supports the small difference between the spectra of the

bare and tagged clusters shown in Figure 4, that suggests the isomer distribution change

does not occur by the tagging and the same isomer type is the spectral carrier in both the

cases.   The remarkable shift of the peak position of the H-bonded OH band with the

tagging would be attributed to the excitation energy dependence of the predissociation

yield in the bare cluster. While the predissociation yield upon the OH band excitation

would be unity in the tagged cluster (in the tag-evaporation channel), that of the bare

cluster can increase with increasing vibrational excitation energy. This is because the

binding energy of the H-bond is much higher than the van der Waals bond with the tag

and assistance by thermal energy is often requested for predissociation upon excitation

of low frequency bands.

4. *n*= 5 cluster

In the observed spectrum of the bare cluster of *n* = 5, the spectral features are similar to

those of *n* = 4 though the peak position of the H-bonded OH stretch band is shifted to

~3200 cm^{-1}. The free OH band position (3676 cm^{-1}) does not show remarkable

difference. The present observed spectrum of the bare cluster is essentially identical to

that reported by Chang *et al*. under their high nozzle temperature and low stagnation

pressure condition. [37, 38] Chang *et al*. have assigned the observed spectrum to an **L** type

isomer. Moreover, they have found that weak bands newly appear at the free OH

(3647 cm^{-1}) and H-bonded OH (3451 cm^{-1}) regions with the lowering nozzle

temperature and increasing the stagnation pressure. They have attributed these bands

to more stable **C** isomers, which are populated by the fall of the cluster temperature.

The characteristic band of the **C** isomer at 3451 cm^{-1} is attributed to the stretching

vibration of the OHs bound to the AA site in the H-bonded ring. This is a marker band

of the H-bond ring formation in H^{+}(MeOH)$_n$.

With the tagging, the spectrum of the $n = 5$ cluster shows very remarkable changes. With the Ar tag, two prominent bands are seen at 3643 and $\sim \sim$3450 cm^{-1}, and these bands agree with those assigned to the **C** isomer in the observation by Chang *et al.* [37, 38] While the population transfer from **L** to **C** is estimated to be only ~10 % in the observation by Chang *et al.*, the Ar (and also N_2) tagging achieved 100 % switching of the population. The N_2 tagged spectrum is very similar to the Ar tagged spectrum. This shows the exclusive population the **C** type isomer with the N_2 tagging. On the other hand, the spectrum of the Ne tagged cluster is clearly different from those of the Ar and N_2 tagged clusters. Two bands (3678 and 3644 cm^{-1}) are seen in the free OH stretch region. The former well agrees with that of the bare cluster (**L** type isomer) and the latter coincides with the Ar tagged cluster (**C** type isomer). Here we note that the free OH in the **L** isomer is an A site while that in the **C** isomer is an AA site, as seen in Figure 2. Thus, the free OH stretch frequencies of these two sites are slightly different from each other. In addition, the spectrum with the Ne tag shows a prominent peak of the H-bonded OH stretch band at ~3100 cm^{-1}, which is similar to the peak in the bare cluster. Therefore, the spectrum with the Ne-tag is reasonably interpreted by the coexistence of the **L** and **C** isomers.

The Q-HSA simulation of $n = 5$ is shown in Figure 3. In $n = 5$, the most

stable structure is the **C** type, and its distribution is predominant in $T \leq \sim 125$ K. The **L** type isomer is, however, more flexible and has lower frequency intermolecular vibrational modes. Therefore, in contrast with the case of $n = 4$, the distribution of the **L** type isomer increases with the elevation of temperature because of the entropy factor. At ~ 125 K, the relative distribution is inverted, and in $T \geq \sim 170$ K, the **L** type isomer becomes dominant. As seen in Figure 4, the observed spectrum of the bare cluster well agrees with the simulation of $T = 200$ K, which is exclusively attributed to the **L** type isomer (as for more detailed comparison among the observed spectra and the temperature-dependent simulation, also see the Electronic Supplementary Information). The finite temperature of the bare cluster is due to the large excess energy in the formation of the protonated cluster. Even with the jet expansion, the cluster cannot be cooled down to the most stable **C** isomer, but takes the **L** type structure with the remaining vibrational energy. On the other hand, the spectra of Ar and N_2 tagged clusters are reproduced by the simulation of $T \leq \sim 70$ K, which is due to the neat **C** type isomer (see the Electronic Supplementary Information). The complete switching of the isomer distribution with the Ar and N_2 tagging is explained by the fall of the cluster temperature, which is essentially the restriction of the total vibrational energy by the weak intermolecular bond. The estimated upper limit of the temperature (T_{max}) of the

21

Ar-tagged cluster is 56 - 91 K (for details, see the ESI). This T_{max} evaluation is well

consistent with the observed isomer distribution of the tagged clusters.

On the other hand, only the Ne tagged clusters shows the coexistence of the **C**

and **L** isomers. This corresponds to the temperature at 100~150 K in the Q-HSA

simulation. However, the binding energy with Ne is reasonably expected to be smaller

than those with Ar or N_2. The T_{max} evaluation also predicts 46 - 81 K for the Ne

tagged cluster, which is lower than the Ar tagged cluster. This suggests that a part of

the Ne tagged clusters is trapped at the local minimum (**L** isomer) and is vibrationally

cooled within the minimum as shown by its sharp vibrational bands. The quite similar

anomaly of the isomer distribution in the tagging has been found for $H^+(H_2O)_n$ ($n = 6, 7,$

and 22). [32-35] The property and origin of this anomaly will be discussed in Section IV.

8.

5. $n = 6$ cluster

In the observed spectrum of the bare cluster of $n = 6$, the further shift to higher

frequency is seen for the H-bonded OH stretch bands and a free OH band appears at the

same position (3677 cm^{-1}) as that in $n = 4$ and 5. With the tagging, in contrast to the

case of $n = 5$, the spectral changes seem to be much less remarkable except the band

narrowing. It is worth to note that the free OH stretch band with the Ar and Ne tags

shows the same frequency (3676 cm^{-1} in both the tags) as that of the bare cluster. Since the complete isomer distribution switching occurs with the tagging at $n = 5$, the spectral behavior of $n = 6$ upon the tagging, that suggests no remarkable isomer distribution change, seems surprising at glance.

The Q-HSA simulation, however, strongly insists the complete isomer distribution switching with the tagging and it well reproduces the observed spectra. In $n = 6$, the **Ct** type is the most stable isomer and its distribution is dominant in $T \leq {\sim}150$ K. With the elevation of temperature, the distribution of the **L** isomer occurs because of the entropy factor and it becomes dominant in $T \geq {\sim} 200$ K. As shown in the IR simulation in Figure 4, the IR spectra of the **Ct** (50 K) and **L** (200 K) isomers are very similar to each other both in the free and H-bonded OH regions. Here we note that the free OH of the **Ct** isomer in its "tail" moiety is an A site, and therefore its stretch frequency is essentially the same as that of the **L** isomer. This is contrast with the case of $n = 5$, in which the free OH site in the **C** isomer is an AA site and its frequency is clearly different from that of an A site in the **L** isomer. In addition, the strong H-bonded band at 3200 - 3400 cm^{-1} shows the clear shoulder with the tagging and it disappears in the bare cluster. This change of the band shape is well reproduced by the simulation, and this agreement supports the Q-HSA simulation.

An interesting issue in $n = 6$ is that the isomer distribution anomaly with the Ne tagging is not seen. The spectrum of the Ne tag totally agrees with that the Ar tag. Though minor contribution of the **L** isomer is not excluded with the Ne tag, it cannot be major as in the $n = 5$ cluster.

6. $n = 7$ and 8

The isomer distribution of $n = 7$ and the influence of the tagging has been reported in our previous paper, except the results of the N_2 tagging. [7] Then, here we only briefly summarize the results. In $n = 7$, the most compact **bC** type isomer is the most stable. The spectral signature of the **bC** type isomer is the disappearance of the free OH stretch band. While the bare cluster shows a weak free OH band (in the bare cluster, the weakening of the free OH band with increasing n is reasonably explained by decrease of the number ratio of the free OH relative to H-bonded OHs), it disappears in all the tagged clusters. In addition, strong H-bonded OH bands, which are marker bands of the H-bonded ring formation, newly appear at 3400 - 3500 cm^{-1} with the tagging. All these changes suggest that the drastic isomer distribution change with the tagging. The Q-HSA simulation demonstrates that the tagged spectra are well reproduced by the cold spectrum at $T \leq \sim 70$ K, in which the **bC** type isomer is predominant while the bare cluster agrees with the higher temperature spectra of $T \geq \sim 150$ K, being consistent of the

L and **Ct** isomers.   Therefore, we observe the closing (**bC** formation) of the totally

open (**L**) or partially open (**Ct**) H-bond networks with the tagging (fall of vibrational

temperature).   We also note that all the tag species show essentially the same spectra.

The $n = 8$ cluster also shows quite similar results to the $n = 7$ cluster.   With the

tagging, the disappearance of the free OH band and appearance of new H-bonded OH

bands occur.   The Q-HSA simulation for $n = 8$ shows the result parallel to that of $n =$

7.   The most stable isomer is the **bC** type, and its distribution is dominant at low

temperature of $T \leq \sim 70$ K.   The distribution of the **Ct** and **L** type isomers occurs with

the elevation of temperature.   The observed spectra with the Ar and N_2 tags are well

reproduced by the simulation at $T \leq \sim 70$ K, and the spectrum of the bare cluster agree

with that at $T = \sim 150$ K.

7.   General trend of temperature dependence

The present systematic study through the observed size range ($n = 4$ -8) clearly

demonstrates a general trend of the temperature dependence of the microscopic H-bond

networks of protonated methanol. The open (unfolded) networks are formed in the bare

cluster because of the excess energy upon the protonation and cluster formation.   In the

other words, the bare cluster is warm ($T = \sim 150$ to 200 K) under the present ion source

condition and the entropy factor determines the preferred network structure.   With the

tagging, temperature of the cluster is limited by the weak intermolecular bond with the tag ($T \leq \sim 70$ K), and the H-bond network is switched to the more compact (folded) forms, which are stabilized by greater number of H-bonds and they are preferred by the enthalpy factor.

A remarkable feature found in the present observation is that the complete switching between the populated isomer types occurs with the tagging (vibrational cooling) in the clusters of the size range of $n = 5 - 8$. This contrasts with the case of protonated water clusters $H^+(H_2O)_n$ at the same size region. [34] Though the Ar tagging also changes IR spectra of $H^+(H_2O)_n$, the magnitude of the isomer population change is much less ($n = 6$ and 7) or almost negligible ($n = 5$ and 8). This difference might be attributed to close competition among the multiple isomers and high relative energy of the flexible (chain type) isomers in protonated water clusters. [16, 58] Both of these two origins come from the strong preference of multiple H-bond coordination of water. The striking contrast with protonated water demonstrates the advantage of protonated methanol as a benchmark to study temperature dependence of H-bond networks.

The observed transformation of the H-bond networks of methanol from the rigid one to the flexible one with elevation of temperature well corresponds to melting in bulk. This temperature dependence is obviously governed by the free energy (balance

between enthalpy and entropy), and the dominant isomer switching can be regarded as phase change in the microscopic scale.   We should, however, be careful in a simple extrapolation of the cluster results to bulk. In a supersonic jet expansion, employed in the present experiment, thermal equilibrium among all the degrees of freedom might not be achieved. It has been well known that translational, rotational, and vibrational temperature is generally different in a supersonic jet expansion because of the different collisional energy transfer efficiency among these characteristic motions. Since the structural isomer distribution is governed mainly by vibrational motion on the potential hypersurface, we focus only on the vibrational temperature to interpret the observed IR spectra.   The good agreement between the observed and simulated IR spectra justifies the present strategy. However, thermal equilibrium between rotational and vibrational motions might change the temperature dependence of the isomer population as suggested by the simulation by Fiften *et al*. in which all the degrees of freedom are counted in the partition function, [45] though the present experimental observations under the supersonic jet condition are not suitable to test the effect of rotational degree of freedom on the isomer distribution.

We also need to note that the excess proton brings the extra complexity (existence of the **bC** type isomers) to the H-bond networks of methanol. Though the

27

H-bond network of protonated clusters will practically converge to those of neutrals in larger sizes, [59] temperature dependence of neutral clusters should be different from that of protonated clusters in the small size.

8. The origin of the anomaly in the tagging

In the present study, we demonstrated that the inert gas tagging cools down the protonated methanol clusters and the predominant distribution of the most stable isomer can be achieved. The case of the Ne tagging of $n = 5$, however, seems to be exceptional. The higher energy **L** isomer coexists with the most stable **C** isomer. This is contrast with the Ar or N_2 tagging, in which the most stable **C** isomer exclusively populates. This phenomenon is quite similar to those found in the tagging of protonated water clusters $H^+(H_2O)_n$. [32-35] Both of $H^+(MeOH)_n$ and $H^+(H_2O)_n$ show the same characteristics for their anomaly in the isomer selectivity with the tagging; (i) The anomaly occurs at specific cluster sizes. (ii) The Ne tag (or H_2 tag) tends to result in coexistence of multiple isomers. (iii) The Ar tag tends to result in a single isomer (we should note that some examples of higher energy isomer preference have also been found for Ar tagging). [4, 30, 31, 36] (iv) The N_2 tag is similar to the Ar tag (in $H^+(H_2O)_6$, weak coexistence of the isomers was observed though the major isomer was the same as the Ar tag). [32] (v) When both the Eigen and Zundel type isomers are possible (in

$H^+(MeOH)_5$, **L** is the Eigen type and **C** is the Zundel type isomer, respectively), the Zundel type isomer is preferred by the Ar tagging (as for this point, in both $H^+(MeOH)_n$ and $H^+(H_2O)_n$, the Zundel type is the most stable isomer in the sizes anomaly has been found, and it is not necessarily clear whether the Zundel type geometry is important or not).

It is clear that the simple energetics cannot explain the anomaly in the isomer selectivity since the binding energy with Ne is expected to be lowest among these three tag species in the present work (this is proved by T_{max} evaluation of $n = 5$ shown in Sec.IV.4 and Electronic Supplementary Information). Therefore, a kinetic factor in the cluster formation process would be a plausible candidate for the origin of the anomaly. Recently, for the pick-up type ion source experiment, the DFT/MD simulation has demonstrated the importance of the kinetic trap for the high energy isomer production with Ar tagging, though this result cannot be directly applied to the present anomaly because of the different cluster generation mechanism.[31]

Third body collisions with the carrier gas should be the major process in the cooling of the cluster in a jet expansion. Therefore, if the kinetic trap at a local minimum (higher energy isomer structure) during the cooling process is essential for the observed anomaly in the tagging, carrier gas dependence is reasonably expected. Then,

we tested some mixture gases (95 % carrier and 5 % tag species) to separate the roles of the tag and the third body collision for cooling.

Figure 6 shows the IR spectra of the bare and tagged $H^+(MeOH)_5$ clusters produced under the various jet expansion conditions. The H_2, Ar, and N_2 tagging (spectra (b), (c), and (f), respectively) was performed by the common carrier gas (95 % He). (The Ne tagging was successful only with the expansion of high pressure neat Ne carrier gas). However, these three spectra show different features. The H_2 tag spectrum is the same as the Ne tag spectrum (100% Ne carrier) and indicates the coexistence of the **C** and **L** type isomers, while the Ar and N_2 tag spectra are exclusively due to the **C** type isomer. In addition, the three spectra of the Ar tagged cluster (spectra ((c) - (e)) showed that the isomer distribution of the tagged cluster is not largely influenced by the carrier gas and stagnation pressure (differences of the bandwidths and H-bonded band intensity, and appearance/disappearance of some minor peaks suggest the vibrational temperature (contribution of hot bands) would somewhat depend on these factors). These experimental results demonstrate that the carrier gas (i.e., third body collision) is not an essential factor of the anomaly in the tagging. Therefore, if a kinetic factor is the key in the anomaly, the tag atom (molecule) is not a specter but it should play a crucial role in the isomerization process during the cooling. A possible

scenario is that the binding energy with the tag becomes the upper limit of the thermal energy from the early stage of the cooling process and isomerization to the minimum energy isomer tends to be prevented in the case of weakly bound tags. [31] Along with such a scenario, the final isomer distribution might be determined by the balance between the isomerization barrier and the binding energy with the tag, and this may cause the remarkable size dependence of the anomaly. We note that the binding energy with the tag also varies with the isomerization of the H-bond network structure. Its quantitative evaluation is not simple and is beyond the scope of this paper.

Finally we also note that the spectra of the bare cluster (spectra (g) − (i)) are similar to each other, and no isomer distribution change is practically seen with the stagnation pressure and carrier gas changes. The influence of the stagnation pressure and carrier gas is limited to relatively small change of the vibrational temperature of the cluster. In comparison to these factors, the influence of the tag is much more significant to tune the isomer distribution though a part of the mechanism is still unclear.

V. Summary

In the present study, the preferential H-bond network structures of $H^+(MeOH)_n$ were

studied by IR spectroscopy of the OH stretch region in conjunction with the DFT simulations of the temperature dependence of the isomer distribution and IR spectra. The significant change of the IR spectra of the clusters of $n \geq 5$ occurred with the inert gas tagging, and it was well interpreted in terms of the fall of the temperature, which induces the switching of the isomer distribution from the open and flexible types to the closed and compact types. Though there have been some partial demonstrations of such a population change so far, the present study clarified the general trend of the isomer population switching by the systematic search in the wide size range. The temperature dependence of the H-bond network structures of $H^+(MeOH)_n$, which is driven by the entropy factor, was demonstrated by the good agreement between the experimental and simulated IR spectra.

In the tagging of $H^+(MeOH)_n$, the anomalous isomer distribution was observed at $n = 5$. The anomaly has the same characteristics as those recently found in the protonated water clusters. The carrier gas dependence of the anomaly was studied to examine the role of the third body collision. The results denied the important role of the third body (carrier gas) in the anomaly, and this suggested that the tag itself plays a crucial role in the kinetics of the formation processes of the tagged clusters.

ACKNOWLEDGEMENTS

Electronic Supplementary Information (ESI) available: Confirmation of the accuracy of the B3LYP relative energy evaluation. Number of stable isomers of $H^+(MeOH)_n$ optimized with B3LYP/6-31G(d).   IR Spectra of $H^+(MeOH)_4$ with one and two Ar and N_2. Temperature dependence of simulated Spectra of $H^+(MeOH)_n$ ($n = 5 - 8$) and their comparison with bare and Ne/Ar-tagged spectra.   Binding energies of Ar and Ne to $H^+(MeOH)_n$ (n = 3 – 5).

REFERENCES

1. J. C. Jiang, Y. S. Wang, H. -C. Chang, S. H. Lin, Y. T. Lee, G. Niedner-Schatteburg, *J. Am. Chem. Soc.* 2000, **122**, 1398-1410.

2. Y. S. Wang, C. H. Tsai, Y. T. Lee, H. –C. Chang, J. C. Jiang, O. Asvany, S. Schlemmer, D. Gerlich, *J. Phys. Chem. A* 2003, **107**, 4217−4225.

3. D. J. Miller, J. M. Lisy, *J. Am. Chem. Soc.* 2008, **130**, 15393−15404.

4. V. Brites, J. M. Lisy, M. –P. Gaigeot, *J. Phys. Chem. A* 2015, **119**, 2468 − 2474.

5. W. H. Robertson, M. A. Johnson, *Ann. Rev. Phys. Chem.* 2003, **54**, 173−213.

6. D. Bing, T. Hamashima , C. –W. Tsai, A. Fujii, J. –L. Kuo, *Chem. Phys.* 2013, **421**, 1–9.

7. T. Hamashima, Y. C. Li, M. C. H. Wu, K. Mizuse, T. Kobayashi, A. Fujii, J. –L. Kuo, *J. Phys. Chem. A* 2013, **117**, 101−107.

8. R. Shishido, Y. –C. Li, C. –W. Tsai, D. Bing, A. Fujii, J. –L. Kuo, *Phys. Chem. Chem. Phys.* published on web. DOI: 10.1039/c5cp01487e.

9. K. Ohashi, J. Sasaki, G. Yamamoto, K. Judai, N. Nishi, H. Sekiya, *J. Chem. Phys.* 2014, **141**, 21307−1−10.

10. J. –L. Kuo, M. L. Klein, *J. Chem. Phys.* 2005, **122**, 024516-1-8.

11. Y. Luo, S. Maeda, K. Ohno, *J. Phys. Chem. A* 2007, **111**, 10732-10737.

12. D. Gerlich, *Phys. Scr.* 1995, **T59**, 256−263.

13. J. Jasik, J. Zabka, J. Roithova, D. Gerlich, *Int. J. Mass Spectrom.* 2013, **354**, 204−210.

14. S. R. Mercier, O. V. Boyarkin, A. Kamariotis, M. Guglielmi, I. Tavernelli, M. Cascella, U. Rothlisberger, T. R. Rizzo, *J. Am. Chem. Soc.* 2006, **128**, 16938−16943.

15. A. Fujihara, N. Noguchi, Y. Yamada, H. Ishikawa, K. Fuke, *J. Phys. Chem. A* **2009**, 113, 8169 − 8175.

16. N. Heine, M. R. Fagiani, M. Rossi, T. Wende, G. Berden, V. Blum, K. R. Asmis, *J. Am. Chem. Soc.* 2013, **135**, 8266−8273.

17. N. Heine, K. R. Asmis, *Int. Rev. Phys. Chem.* 2015, **34**, 1−34.

18. J. A. Fournier, C. J. Johnson, C. T. Wolke, G. H. Weddle, A. B. Wolk, M. A. Johnson, *Science*, 2014, **344**, 1009 − 1012.

19. A. B. Wolk, C. M. Leavitt, E. Garand, M. A. Johnson, *Acc. Chem. Res.* 2014, **47**, 202−210.

20. C. A. Rice, F. X. Hardy, O. Gause, J. P. Maier, *J. Phys. Chem. Lett.* 2014, **5**, 942−945.

21. S. Dillinger, J. Mohbach, J. Hewer, M. Gaffga, G. Nieder-Schattebrug, *Phys. Chem.*

Chem. Phys. 2015, **17**, 10358-10362.

22. M. Okumura, L. I. Yeh, J. D. Myers, Y. T. Lee, *J. Chem. Phys.* 1986, **85**, 2328-2329.

23. M. Okumura, L. I. Yeh, J. D. Myers, Y. T. Lee, *J. Phys. Chem.* 1990, **94**, 3416-3427.

24. J. M. Headrick, E. G. Diken, R. S. Walters, N. I. Hammer, R. A. Christie, J. Cui, E. M. Myshakin, M. A. Duncan, M. A Johnson, K. D. Jordan, *Science* 2005, **308**, 1765-1769.

25. P. J. Kelleher, C. J. Johnson, J. A. Fournier, M. A. Johnson, A. B. McCoy, *J. Phys. Chem. A* 2015, **119**, 4170−4176.

26. G. E. Douberly, R. S. Walters, J. Cui, K. D. Jordan, M. A. Duncan, *J. Phys. Chem. A* 2010, **114**, 4570-4579.

27. O. Dopfer, *Int. Rev. Phys. Chem*. 2003, **22**, 437−495.

28. M. Schmies, M. Miyazaki, M. Fujii, O. Dopfer, *J. Chem. Phys*. 2014, **141**, 214301-1-17.

29. K. Mizuse, A. Fujii, *Chem. Phys*. **2012**, 419, 2 -7.

30. O. Rodriguez Jr., J. M. Lisy, *J. Phys. Chem. Lett*. 2011, **2**, 1444-1448.

31. V. Brites, A. Cimas, R. Spezia, N. Sieffert, J. M. Lisy, M. −P. Gaigeot, *J. Chem. Theory Comput.* 2015, **11**, 871-883.

32. K. Mizuse, A. Fujii, *Phys. Chem. Chem. Phys.* 2011, **13**, 7129-7135.

33. K. Mizuse, A. Fujii, *J. Phys. Chem. Lett.* 2011, **2**, 2130-2134.

34. K. Mizuse, A. Fujii,   *J. Phys. Chem. A* 2012, **116**, 4868-4877.

35. A. Fujii, K. Mizuse**,** *Int. Rev. Phys. Chem.* 2013, **32**, 266–307.

36. K. R. Asmis, T. Wende, M. Brümmer, O. Gause, G. Santambrogio, E. C. Stanca-Kaposta, J. Döbler, A. Niedziela, J. Sauer, P*hys. Chem. Chem. Phys*. 2012, **14**, 9377-9388.

37. H. −C. Chang; J. −C. Jiang, S. H. Lin, Y. T. Lee, H. −C. Chang, *J. Phys. Chem. A* 1999, **103**, 2941-2944.

38. H. −C. Chang, J. –C. Jiang, H. –C. Chang, L. R. Wang, Y. T. Lee, *Isr. J. Chem*. 1999, **39**, 231-243.

39. A. Fujii, S. Enomoto, M. Miyazaki, N. Mikami, *J. Phys. Chem. A* 2005, **109**, 138-141.

40. J. –L. Kuo, A. Fujii, N. Mikami, *J. Phys. Chem. A* 2007, **111**, 9438-9445.

41. Y. J. Hu, F. B. Fu, E. R. Bernstein, *J. Chem. Phys*. 2006, **125**, 154306-1-5.

42. K. Tono, J.-L. Kuo, M. Tada, K. Fukazawa, N. Fukushima, C. Kasai, K. Tsukiyama, J. Chem. Phys. 2008, **129**, 084304-1-8.

43. E. S. Stoyanov,. I. V. Stoyanova, C. A. Reed, *Chem. Eur. J*. 2008, **14**, 3596 – 3604.

44. J. J. Fifen, M. Nsangou, Z. Dhaouadi, O. Motapon, N. −E. Jaidane, *J. Chem. Theory Comput*. 2013, **9**, 1173-1181.

45. J. J. Fifen, M. Nsangou, Z. Dhaouadi, O. Motapon, N. −E. Jaidane, *J. Chem. Phys*. 2013, **138**, 184301-1-12.

46. Q. −C. Nguyen, Y. −S. Ong, J. −L. Kuo, , *J. Chem. Theory and Comp*. 2009, **5**, 2629-2639.

47. Q. −C. Nguyen, Y. −S. Ong, H. Soh, J. −L. Kuo, *J. Phys. Chem. A* 2008, 112,6257-6261.

48. H. Soh, Y. −S. Ong, Q. −C. Nguyen, Q. Huy, N. M. Salahuddin, T. Hung, J. −L. Kuo, IEEE Trans. Evo. Comp.2010, 14, 419-437.

49. C. C. Wu, J. C. Jiang, D. W. Boo, S. H. Lin, Y. T. Lee, H. −C. Chang, *J. Chem. Phys*. 2000, **112**, 176-188.

50. J. C. Jiang, C. Chaudhuri, Y. T. Lee, H. −C. Chang, *J. Phys. Chem. A* 2002, **106**,

10937-10944.

51. C. C. Wu, C. Chaudhuri, J. C. Jiang, Y. T. Lee, H. –C. Chang, *J. Phys. Chem. A*

2004, **108**, 2859-2866.

52. Y. L. Cheng, H. Y. Chen, K. Takahashi, *J. Phys. Chem. A* 2011, **115**, 5641−5653.

53. M. Morita, K. Takahashi, *Phys. Chem. Chem. Phys.* 2012, **14**, 2797−2808.

54. M. J. Frisch, G. W. Trucks, H. B. Schlegel, G. E. Scuseria, M. A. Robb, J. R.

Cheeseman, G. Scalmani, V. Barone, B. Mennucci, G. A. Petersson, H. Nakatsuji, M.

Caricato, X. Li, H. P. Hratchian, A. F. Izmaylov, J. Bloino, G. Zheng, J. L. Sonnenberg,

M. Hada, M. Ehara, K. Toyota, R. Fukuda, J. Hasegawa, M. Ishida, T. Nakajima, Y.

Honda, O. Kitao, H. Nakai, T. Vreven, J. Montgomery, J. E. Peralta, F. Ogliaro, M.

Bearpark, J. J. Heyd, E. Brothers, K. N. Kudin, V. N. Staroverov, R. Kobayashi, J.

Normand, K. Raghavachari, A. Rendell, J. C. Burant, S. S. Iyengar, J. Tomasi, M. Cossi,

N. Rega, N. J. Millam, M. Klene, J. E. Knox, J. B. Cross, V. Bakken, C. Adamo, J.

Jaramillo, R. Gomperts, R. E. Stratmann, O. Yazyev, A. J. Austin, R. Cammi, C.

Pomelli, J. W. Ochterski, R. L. Martin, K. Morokuma, V. G. Zakrzewski, G. A. Voth, P.

Salvador, J. J. Dannenberg, S. Dapprich, A. D. Daniels, O. Farkas, J. B. Foresman, J. V.

Ortiz, J. Cioslowski and D. J. Fox, Gaussian 09, Revision B.01, Gaussian, Inc.,

Wallingford CT, 2009.

55. D. Bing, T. Hamashima, Q. C. Nguyen, A. Fujii, J. −L. Kuo, *J. Phys. Chem. A* 2010, **114**, 3096-3102.

56. N. Solcà, O. Dopfer, *J. Phys. Chem. A* 2005, **109**, 6174-6186.

57. E. P. L. Hunter, S. G. Lias, *J. Phys. Chem. Ref. Data* 1998, **27**, 413−457.

58. N. Heine, M. R. Fagiani, K. R. Asmis, *J. Phys. Chem. Lett*. 2015, **6**, 2298-2304.

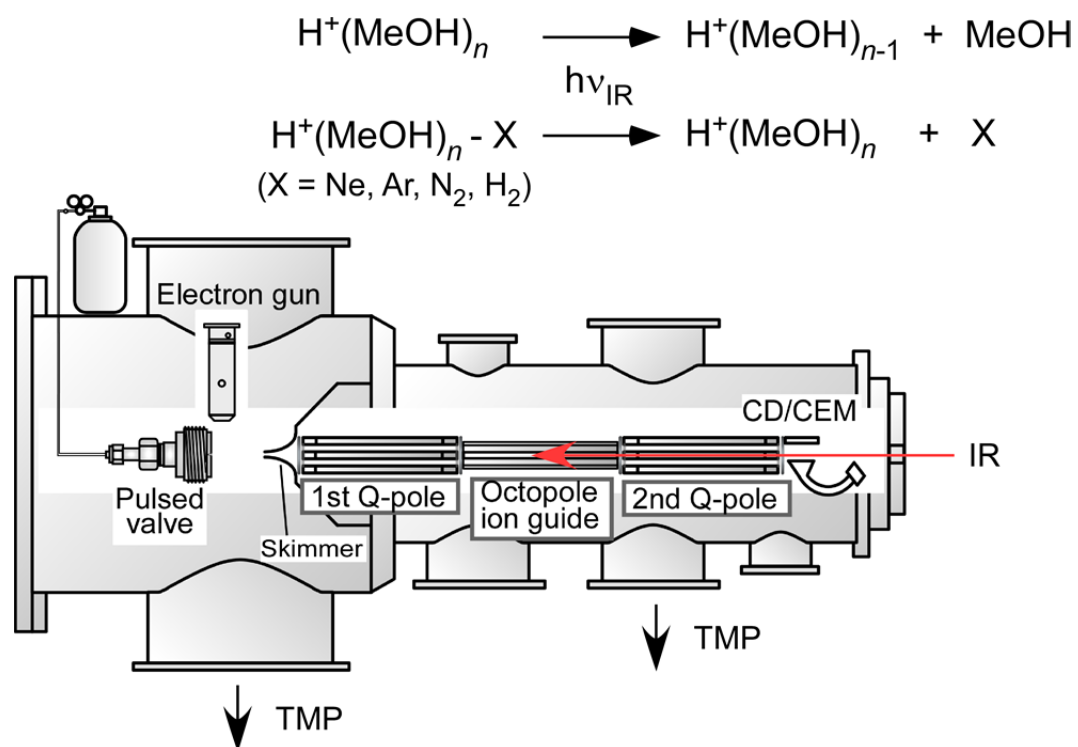59. T. Kobayashi, R. Shishido, K. Mizuse, A. Fujii, J. −L. Kuo, *Phys. Chem. Chem. Phys*. 2013, **15**, 9523-9530.

$$H^+(MeOH)_n \longrightarrow H^+(MeOH)_{n-1} + MeOH$$

$$h\nu_{IR}$$

$$H^+(MeOH)_n - X \longrightarrow H^+(MeOH)_n + X$$

$$(X = Ne, Ar, N_2, H_2)$$

Figure 1 Schemes of the tandem quadrupole mass spectrometer and infrared

photodissociation spectroscopy used in this study. Q-pole = quadrupole mass

spectrometer, CD = conversion dynode, CEM = channeltron electron multiplier, TMP =
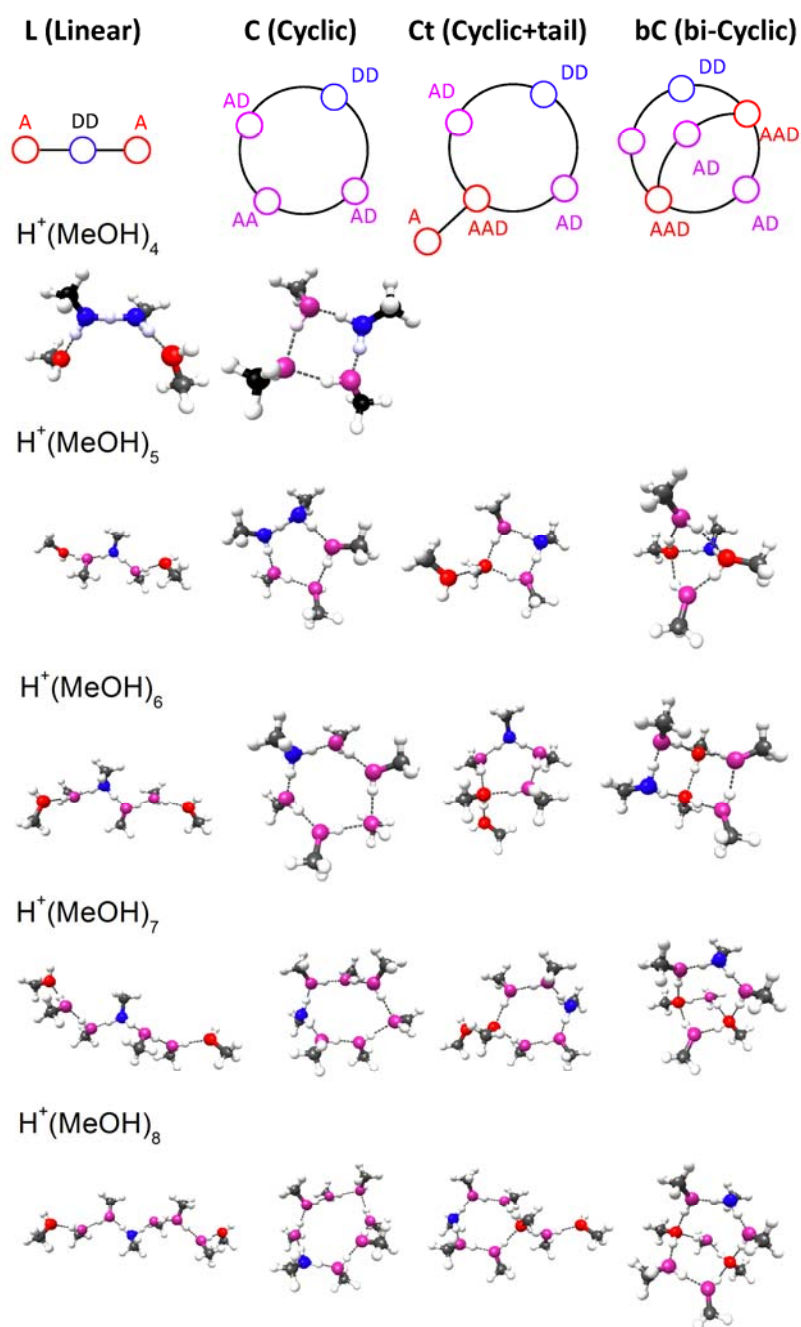
turbo molecular pump.

Figure 2 (Top) Schematic representations of the hydrogen bond network types (**L**, **C**,

Ct, and **bC**) of protonated methanol clusters. Circles represent methanol molecules,

and lines indicate hydrogen bonds. DD (double donor site, ion core), A (single

acceptor site), AA (double acceptor site), AD (acceptor-donor site), and AAD (double

43

acceptor-single donor site).   (Bottom) Structures of the most stable isomers in each

network type.   For easy visualization, oxygen atoms of DD and AD are shown in blue

and pink, respectively.
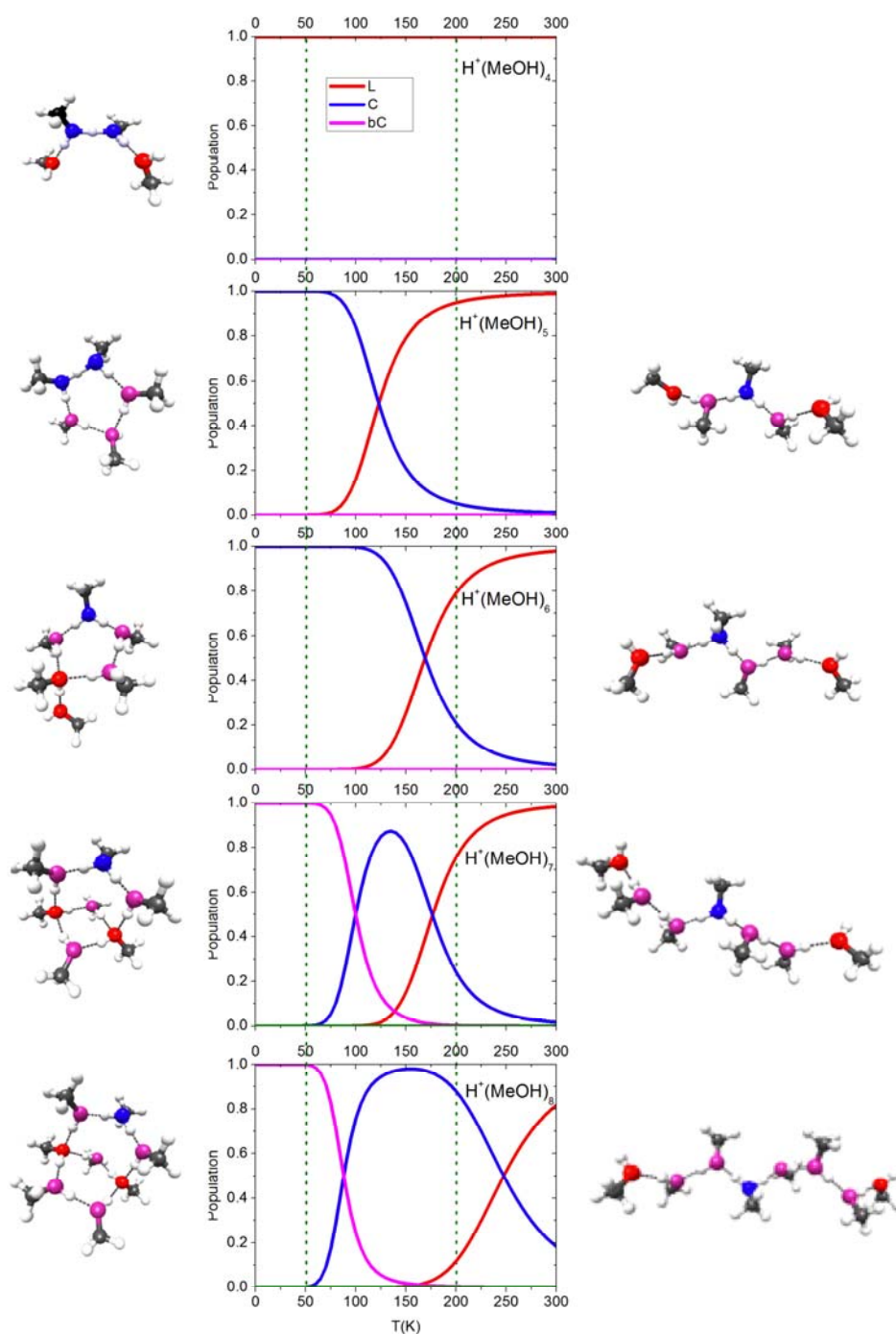
Figure 3 Temperature dependence of isomer type populations of H$^+$(MeOH)$_n$ (n = 4 –

8) calculated by Q-HSA are shown in the center. All the calculations were performed at

B3LYP/6-31+G(d).   The polts of the **C** type isomers (blue lines) include the population

45

of the **Ct** type isomers (see text). Except *n*=4, topology of the dominating species changes with elevation of temperature. In low (~50 K) temperature, the topology is relatively more compact than the topology at high (~200 K) temperatures. On the left panel, we show the structures of the dominating isomer at 50 K. At 200 K, coexistence of many isomers can be found. For a given size, we show only the structure of the isomer with highest population as a representative, on the right panel.
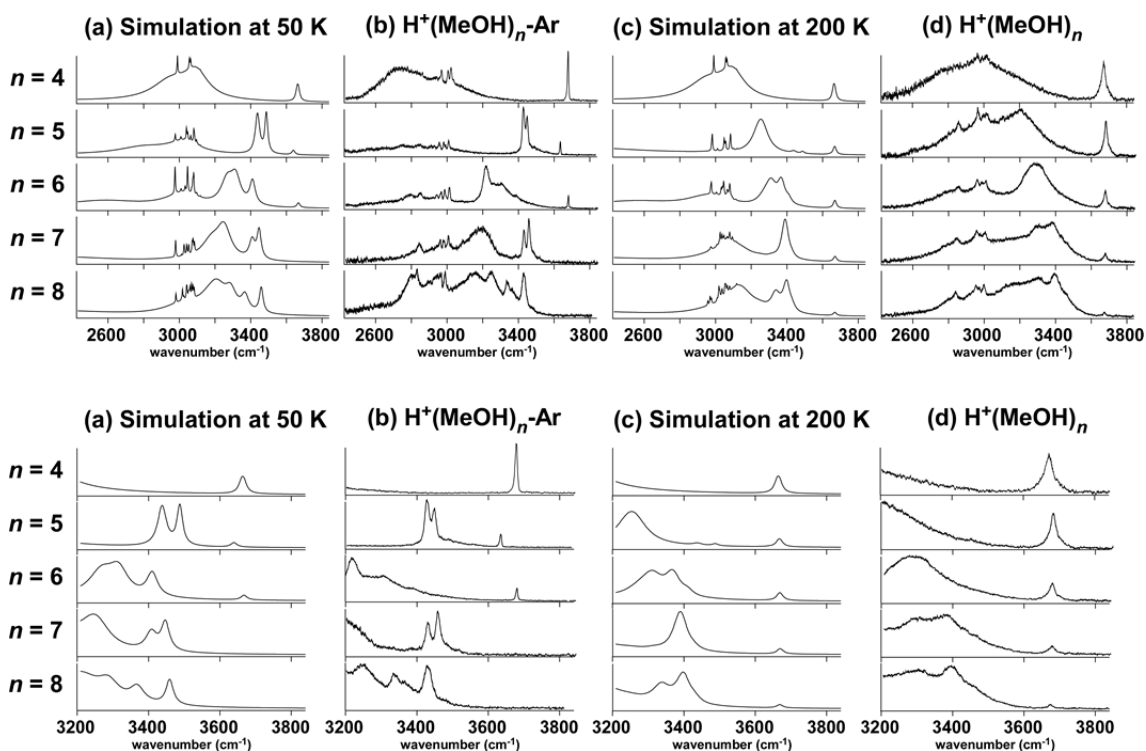
Figure 4 Comparisons on the observed IR spectra of (b) Ar-tagged and (d) bare

$H^+(MeOH)_n$ clusters ($n = 4 - 8$) with the DFT-simulated spectra at (a) 50 K and (c) 200

K respectively. The upper traces show the full frequency region (2430 – 3840 cm^{-1}),

and the lower traces are the expanded plots of the high frequency region (3200 – 3840

cm^{-1}). The spectral simulations were performed at B3LYP/6-31+G(d). Over all,

observed spectra of Ar-tagged species agree well with simulated spectra at lower (~50

K) temperature and observed spectra of bare species resemble simulated spectra at

higher (150~200 K). This finding is in agreement with the expectation that bare clusters
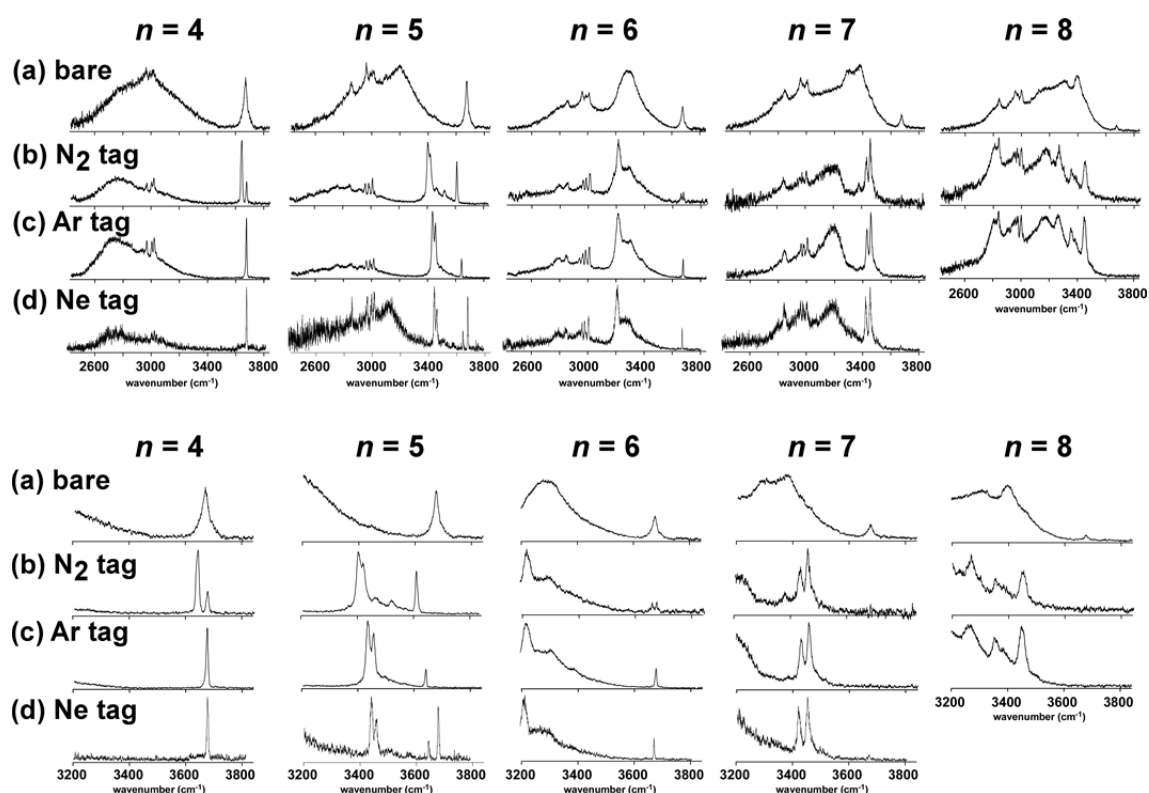
have higher internal energy.

46

Figure 5   IR spectra of the bare and tagged $H^+(MeOH)_n$ clusters ($n = 4 - 8$) in the OH

and CH stretching vibrational region. The upper traces show the full observed frequency

region ($2430 - 3840$ cm^{-1}), and the lower traces are the expanded plots of the high

frequency region ($3200 - 3840$ cm^{-1}).   Carrier gas conditions are as follows; (a) bare

clusters: 95 %He and 5 % Ar, total stagnation pressure 9 MPa, (b) N_2 tagged clusters:

He 95 % and N_2 5%, total stagnation pressure 8 MPa, (c) Ar tagged clusters: 95 %He

and 5 % Ar, total stagnation pressure 9 MPa, (d) Ne tagged clusters: 100 % Ne,
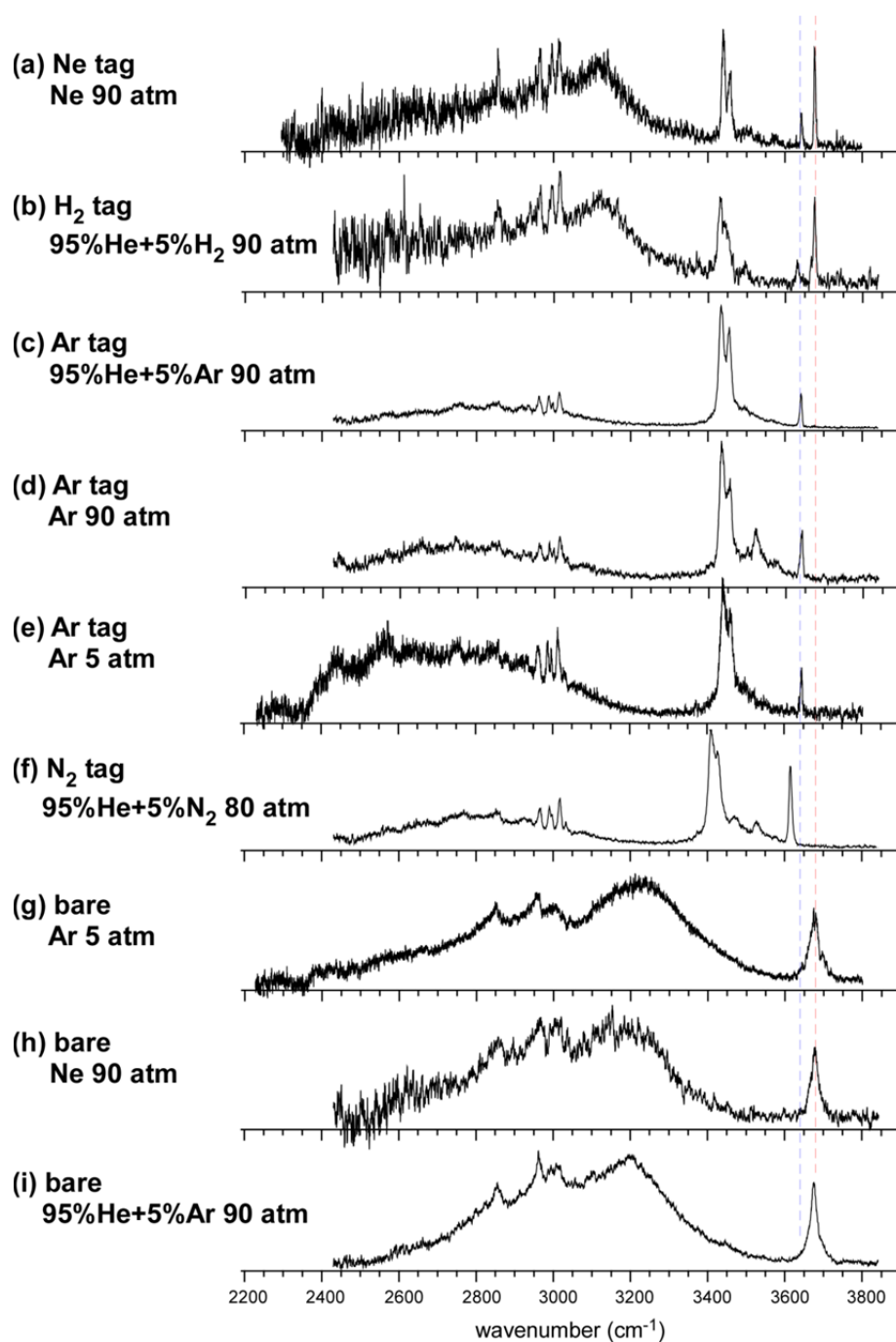
stagnation pressure 9 MPa.

47

Figure 6   Comparison of IR spectra of the bare and tagged clusters of $H^+(MeOH)_5$

produced under the different jet expansion conditions.   Dashed red and blue lines are

eye guides for the free OH bands of the **L** and **C** isomers, respectively.